Laser tracking leader-follower automatic cooperative navigation system for UAVs

Rui Ming[1,2], Zhiyan Zhou[1,3,4*], Zichen Lyu[1,3,4,5], Xiwen Luo[1,3,4,5], Le Zi[1,3,4,5], Cancan Song[1,3,4,5], Yu Zang[1,3,4,5], Wei Liu[1,3,4,5], Rui Jiang[5*]

(1. *College of Engineering, South China Agricultural University / Guangdong Laboratory for Lingnan Modern Agriculture, Guangzhou 510642, China*;
2. *College of Computer and Control Engineering, Minjiang University / Fujian Provincial Key Laboratory of Information Processing and Intelligent Control, Fuzhou 350108, China*;
3. *Guangdong Provincial Key Laboratory for Agricultural Artificial Intelligence (GDKL-AAI), Guangzhou 510642, China*;
4. *Guangdong Engineering Research Center for Agricultural Aviation Application (ERCAAA), Guangzhou 510642, China*;
5. *Key Laboratory of Key Technology on Agricultural Machine and Equipment, South China Agricultural University, Ministry of Education of P.R. China, Guangzhou 510642, China*)

Abstract: Currently, small payload and short endurance are the main problems of a single UAV in agricultural applications, especially in large-scale farmland. It is one of the important methods to solve the above problems of UAVs by improving operation efficiency through multi-UAV cooperative navigation. This study proposed a laser tracking leader-follower automatic cooperative navigation system for multi-UAVs. The leader in the cluster fires a laser beam to irradiate the follower, and the follower performs a visual tracking flight according to the light spot at the relative position of the laser tracking device. Based on the existing kernel correlation filter (KCF) tracking algorithm, an improved KCF real-time spot tracking method was proposed. Compared with the traditional KCF tracking algorithm, the recognition and tracking rate of the optimized algorithm was increased from 70% to 95% in indoor environment, and was increased from 20% to 90% in outdoor environment. The navigation control method was studied from two aspects: the distance coordinate transformation model based on micro-gyroscope and navigation control strategy. The error of spot position was reduced from the maximum (3.12, −3.66) cm to (0.14, 0.12) cm by correcting the deviation distance of the spot at different angles through a coordinate correction algorithm. An image coordinate conversion model was established for a complementary metal-oxide-semiconductor (CMOS) camera and laser receiving device at different mounting distances. The laser receiving device was divided into four regions, S0-S3, and the speed of the four regions is calculated using an uncontrollable discrete Kalman filter. The outdoor flight experiments of two UAVs were carried out outdoors using this system. The experiment results show that the average flight error of the two UAVs on the *X*-axis is 5.2 cm, and the coefficient of variation is 0.0181. The average flight error on the *Z*-axis is 7.3 cm, and the coefficient of variation is 0.0414. This study demonstrated the possibility and adaptability of the developed system to achieve multi-UAVs cooperative navigation.

Keywords: two-UAVs cooperative, visual navigation, laser tracking
DOI: 10.25165/j.ijabe.20221502.6350

Citation: Ming R, Zhou Z Y, Lyu Z C, Luo X W, Zi L, Song C C, et al. Laser tracking leader-follower automatic cooperative navigation system for UAVs edited. Int J Agric & Biol Eng, 2022; 15(2): 165–176.

1 Introduction

Unmanned Aerial Vehicles (UAVs) have been playing an increasingly important role in civilian use in recent decades[1]. Compared with traditional ground machinery, UAVs can be used in chaotic scenes and environments, such as fire and rescue scenes. It can also be used to protect areas from environmental damage and reduce the labor intensity of farmers, such as farmland spray[2,3].

When working on large-scale farmland, UAVs needs to increase their payload and endurance capacity to improve operation efficiency. However, due to the current technical development and regulations, the overall dimensions of UAV have received greater restrictions, making it difficult to increase endurance time and payload[4,5].

In order to solve the payload and endurance problems of a single UAV, two or more UAVs can be used to achieve cluster operations and expand the UAV operating area to improve operating efficiency. So, it is one of the important methods to solve the above problems of UAVs by improving operation efficiency through multi-UAVs cooperative navigation.

Existing cluster methods of multi-UAVs are mainly divided into absolute navigation and relative navigation[6]. The absolute navigation method operates according to the established mission

Received date: 2020-12-08 **Accepted date:** 2021-09-02
Biographies: Rui Ming, Associate Professor, research interests: agricultural aviation, Email: rming@mju.edu.cn; **Zichen Lyu**, Master candidate, research interests: agricultural aviation, Email: zichen_lv@qq.com; **Xiwen Luo**, Professor, research interests: agricultural Equipment, precision agriculture and agricultural aviation, Email: xwluo@scau.edu.cn; **Le Zi**, Master candidate, research interests: information transmission, and intelligent control system, Email: 891750786@qq.com; **Cancan Song**, PhD candidate, research interests: precision agriculture and agricultural aviation, Email: songcc@stu.scau.edu.cn; **Yu Zang**, PhD, research interests: agricultural aviation, Email: zangyu@scau.edu.cn; **Wei Liu**, PhD candidate, research interests: precision agriculture and agricultural aviation, Email: 1341011201@qq.com.
***Corresponding author: Zhiyan Zhou**, Professor, research interests: agricultural aviation. College of Engineering, South China Agricultural University, Guangzhou 510642, China. Tel: +86-13560026139, Email: zyzhou@scau.edu.cn; **Rui Jiang**, Post-doctoral, research interests: precision agriculture and agricultural aviation. College of Engineering, South China Agricultural University, Guangzhou 510642, China. Tel: +86-20-38676975, Email: ruiojiang@scau.edu.cn.

objectives and uses the Global Navigation Satellite System (GNSS) or Real-Time Kinematic (RTK) system for multi-UAV formation flight[7,8]. Due to the narrow bandwidth of the GNSS loop, the vulnerability to interference, and the low receiver data update rate, it is difficult to meet the requirements of real-time measurement and control. The RTK system can meet the requirements of flight in multi-UAV coordination, and it has the advantages of strong autonomy, small size, and continuous output information. However, the cost is relatively high, and the corresponding ground base station and air positioning equipment should be equipped at the same time.

There are two main ways of relative navigation: communication navigation and visual navigation. In communication navigation, that is, the UAV acquires position and attitude information based on its high-precision sensors and uses wireless transmission modules to conduct relevant information interaction to fulfill the user's task requirements[9,10]. Typical communication navigation is based on the leader-follower-based method[11], which advantage is that strong damage resistance and high intelligence. However, the disadvantage of communication navigation is that when the number of UAVs increases, the computational load of information and the communication delay between UAVs will also increase at the same time, finally reducing the robustness of the UAV cluster.

Visual navigation has become a hot research topic in the UAV cluster because visual sensors can provide abundant information[12]. Tang et al.[13,14] used thermal imaging cameras and visible light cameras to track the UAV under different lighting and brightness conditions, respectively. Lin et al.[15] used the monocular camera to extract the UAV features and used the algorithm cascade classifier to classify the features in different situations. Vetrella et al.[16] combined visual navigation and carrier phase differential navigation to improve UAV attitude estimation in real-time or post-processing. In the study of Gassner et al.[17], a leader-follower mode of dual UAV carrier flight was proposed by using a monocular camera without explicit communication. The above visual tracking system takes UAV as the target feature, which can achieve good tracking effects in various applicable scenarios, but it is difficult to effectively track the target in the case of large illumination changes or complex environmental characteristics.

The laser has been widely used in military, medical, navigation, and other fields due to its advantages of high energy, accurate orientation, and high uniformity[18]. Walter et al.[19] proposed an onboard relative localization method, based on ultraviolet light, used for real-time control of a leader-follower formation of multi-UAVs. This method realizes the cooperative flight of multi-UAVs through ultraviolet light and camera, but it has obvious shortcomings. According to the experiment results, the followers make simple harmonic motions according to the leader's position during the tracking process, and the maximum error distance between the two UAVs is 6 m. When the number of followers increases, simple harmonic motion among followers may cause collisions, and thus security needs to be improved, it is difficult to deploy in practical applications. Park et al.[20] used infrared light (850 nm) emitting diode to strengthen the reflection of the guide label installed on the leader, installs an infrared camera from the follower and follows the movement of the guide label on the leader. The infrared light used in this method can effectively reduce the impact of sunlight. However, because it is a low-power LED, it can only track two units at a short distance. Therefore, in view of the above problems of large flight error distance and low power of emission light source, combining the existing visual navigation technology and the advantages of laser tracking navigation, we proposed a multi-UAV visual navigation device based on laser tracking.

In order to reduce the tracking error caused by communication navigation, a visual camera was used in this study to measure the relative distance between two UAVs. To reduce the failure rate of visual tracking, the laser is used instead of the UAV as the tracking feature in visual perception. To achieve robust visual tracking of an autonomous system, an improved kernel correlation filter (KCF) real-time spot tracking method is designed. The tracking method can estimate laser spot position coordinates under reliable visual feedback, and convert them into the flying speed of the UAV, so as to realize the synchronous tracking flight of two UAVs.

Figure 1 illustrates the laser tracking leader-follower automatic cooperative navigation system. In this system, the UAV equipped with the laser transmitting device serves as the team leader, which provides a laser spot as the follower's tracking target. The rest of the UAV is a follower, which follows the laser spot's location and flies synchronously with the leader. To avoid danger, a minimum safe distance was set between the two UAVs. During the flight, airborne sensors such as optical flow and ultrasound only play space positioning, and there was no communication between the two UAVs, all the calculations are performed separately on the two UAVs.

1. Leader UAV 2. Follower UAV 3. Laser emitting device 4. Laser receiving device 5. CMOS camera 6. Visual processing device 7. Laser beam
Note: COMS: Complementary metal-oxide-semiconductor.

Figure 1 Schematic diagram of Two-UAV automatic navigation device based on optical tracking

Based on the existing visual navigation technology and laser navigation, a visual tracking method and device based on laser tracking were proposed. The differences between the navigation of this study and the existing navigation are listed in Table 1.

In addition to the above differences with the existing navigation methods, this study also proposed an improved real-time KCF spot tracking method, which can accurately identify the spot position under different illumination conditions. And a navigation control method was proposed to automatically correct the position coordinates of the light spot according to the angle information provided by the micro gyroscope and convert the image coordinates into flight coordinates. Compared with the existing visual navigation system, the laser tracking automatic navigation system has higher tracking accuracy and more robust visual method in multi-UAV cooperative navigation.

2 Framework of the system

The system proposed in this study is mainly composed of three parts: the first part is the laser transmitting device on the leader, the second part is the laser receiving device on the follower, and the third part is the laser recognition device on the follower as shown in Figure 1.

Table 1 Differences between the navigation of this study and the existing navigation

Navigation methods	Characteristic
Absolute navigation[7,8]	1) Strong autonomy, small size, and continuous output information; 2) Narrow band width of the GNSS loop, the vulnerability to interference, and the low receiver data update rate; 3) Cost is relatively high, and the corresponding ground base station and air positioning equipment should be equipped at the same time.
Communication navigation[11]	1) Strong damage resistance and high intelligence; 2) Low robustness due to the limited communication transmission bandwidth and a large amount of data interaction; 3) The tracking error will be propagated backward step by step and amplified.
Visual navigation[12]	1) The number of UAVs in the cluster can be expanded and low communication; 2) Visual sensors can provide more abundant information; 3) It is difficult to effectively track the target when the illumination brightness changes greatly or the surrounding environment is complex.
Laser navigation[19,20]	1) High energy, accurate orientation, and high uniformity; 2) Security needs to be improved and hard to deploy in practical applications. 3) Maximum error distance is 6 m and makes simple harmonic motion between the two UAVs
The navigation proposed in this study	1) Do not rely on GPS/RTK for positioning, and realize tracking flight through onboard sensors; 2) There is no communication between the two UAVs, which effectively avoids the movement deviation caused by limited communication navigation bandwidth and massive data interaction; 3) Using laser spot as visual recognition target can effectively avoid the influence of complex environment; 4) High tracking accuracy.

During the flight, the UAV equipped with laser transmitting device is named a team leader, while the UAV equipped with laser receiving device is called 'follower'. The flying mode of the leader can be controlled manually or fly according to the preset route. Before take-off, the laser tracking system on the follower needs to complete initialization. After the two UAVs take off, the leader turns on the laser transmitting device and fires a laser beam to the followers' laser receiving device. The laser recognition device on the follower starts to collect the spot image on the laser receiving device and obtains the position information of the laser spot. The onboard computer uses the navigation control method to convert the laser spot position information into the UAV's flying speed and transmits it to the flight controller. The follower flies according to the flying speed, and realizes the simultaneous flight of the two UAVs through laser tracking. The working principle of the device is shown in Figure 2. The main control parameters of the device are listed in Table 2.

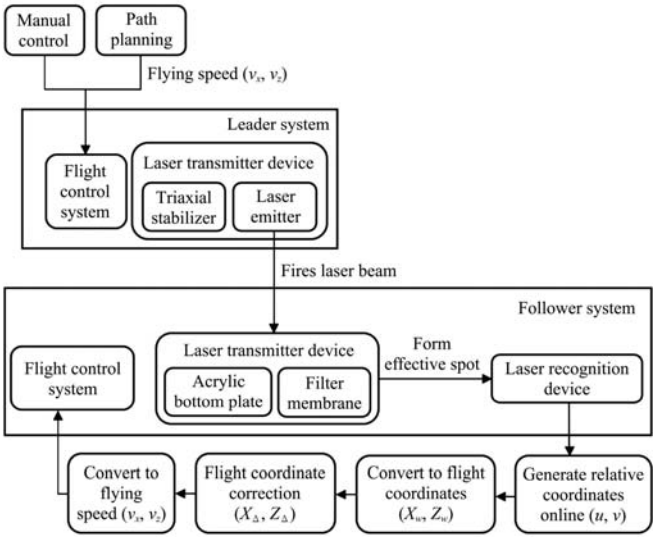

Figure 2 Working principle of the laser tracking navigation system

The laser transmitting device mainly includes a laser stabilization module and a laser-beam module. The laser stabilization module uses the STORM32BGC three-axis brushless stabilizer, effectively reducing the laser emission module's jitter during the UAV flight. The laser-beam module is installed on the stabilizer, equipped with a 500 mW power red laser transmitter, and the battery is equipped with a 3.7 V (1800 mAh) lithium battery. The laser-transmitting device's function is to transmit a laser beam perpendicular to the flying direction of the leader. The leader guides the follower to follow the flight through the laser beam to realize the leader-follower simultaneous flight.

Table 2 Main control parameters of the laser tracking navigation system

Variables	Meaning
u	X-axis pix coordinates of the laser spot
v	Z-axis pix coordinates of the laser spot
X_w	X-axis flight coordinates of UAV
X_z	Z-axis flight coordinates of UAV
X_Δ	X-axis flight coordinates of UAV after correction
Z_Δ	Z-axis flight coordinates of UAV after correction
v_x	X-axis flying speed of UAV
v_z	Z-axis flying speed of UAV

The laser receiving device includes a laser receiving plate and a light-transmitting film. The laser receiving board is a 2 mm polyvinyl chloride (PVC) board, and the laser can form effective reflection and transmission on the receiving board. SunMaster's sr-space silver high-definition filter film was selected as the light-transmitting film and pasted on the PVC board to form a clear and effective light spot on the PVC board. The laser receiving device's function is to receive the laser beam transmitted from the leader and form an effective recognizable spot on the receiving board, waiting for the laser tracking device's recognition and tracking.

The laser recognition device consists of a complementary metal-oxide-semiconductor (CMOS) camera and an onboard computer. Choose OpenMV4 H7 for the CMOS camera. The Raspberry Pi 3B+ was selected as the micro airborne computer. Since the CMOS camera uses a fixed focus lens, different installation positions can affect the laser receiving device's spot acquisition range. To achieve the most complete and comprehensive collection of the spot information on the laser receiving device by the CMOS camera, the best installation position is chosen between the camera and the laser receiving device. The laser recognition device's function is to first collect the effective light spot on the laser receiving device in the form of a video stream and then obtain the image coordinates of the light spot through a visual processing algorithm. The second step uses the coordinate conversation model to convert the image coordinates of

the laser spot into the flying speed of the follower. Finally, the navigation system controls the follower to fly synchronously according to the acquired flying speed. Table 3 provides details of the materials and equipment used in the system.

Table 3 Details of the materials and equipment for laser tracking navigation system

Material	Parameters
STORM32BGC	Processor: STM32F103RC Maximum jitter Angle: 1 degree Gyroscope sampling frequency: 700 Hz
Red laser	Power: 500 MW Working voltage: 2.8-5.2 V (DC) Wavelength: 650 nm
PVC plate	Thickness: 2 mm
Filter film	Transmittance: 18% Reflectivity: 85%
OpenMV4 H7	OV7725 sensor 640×480 16-bit RGB565
Raspberry Pi 3B+	CPU: ARM Cortex-A53 1.4 GHz SOC: Broadcom BCM2837

It can be seen from the above that the main research content of this article has three points: Firstly, when the laser spot is irradiated on the laser receiving device, the method of identifying and obtaining the position of the spot. Secondly, after obtaining the position of the light spot, the method of accurately converting the position of the light spot into the flight coordinates of the UAV. Thirdly, the method of converting the UAV's flight coordinates into the flying speed of the UAV. Through the research of these three parts, the position of the laser spot transmitted from the leader can be converted into the follower's flying speed, realize the tracking of the spot position by the follower, and finally achieve the simultaneous flight of two UAVs.

3 Visual tracking method

When the laser irradiates the laser receiving device from a laser spot, the CMOS camera needs to locate and track the spot position after obtaining the image. In most cases, images acquired by a CMOS camera adopt the RGB color space, but it is sensitive to light brightness and is not suitable for image analysis with a large range of illumination variations[21]. However, the HSV color space is relatively intuitive and has a strong anti-interference ability to light and other effects[22]. Therefore, the color space conversion of the video image from RGB to HSV is carried out first.

With the maturity of machine learning algorithms, discriminant methods are becoming more and more common in the field of target tracking[23]. To achieve high robustness and longtime tracking, an improved KCF real-time spot tracking method is proposed. The discriminant method's main idea is to score the confidence of different sub-areas in the search area by the classifier and identify the target's location by analyzing the response strength layer. As a discriminant tracking method of typical nuclear correlation filtering, KCF has achieved remarkable accuracy and efficiency[24]. However, in the process of using KCF, if the target is affected by the change of illumination brightness, interference of similar targets, and other factors, the target will still be lost.

The KCF tracking algorithm's main idea to train the displacement filter is to learn a discriminant correlation filter to locate a new frame's target. In this study, a scale filter was added based on a displacement filter, and the scale pyramid was used to extract target samples. The sparse matrix was used to carry out cyclic sampling in the target region to improve the algorithm's computational efficiency and tracking accuracy. In the algorithm, ridge regression was used to obtain the optimal correlation filter h_i (Equation (1)).

$$\varepsilon = \sum_{i=1}^{t} \| h_i \times x_i - g_i \|^2 + \lambda \| h_i \|^2 \tag{1}$$

where, x_i is the extraction of the number i training sample; g_i is the target output of the number i training sample; λ is a regular term of a polynomial to prevent overfitting; h_i is the optimal correlation filter of the number i training sample.

According to Parseval's theorem, the operation is converted to the frequency domain as Equation (2).

$$\min \frac{1}{MN} \{ [\sum_{i=1}^{t} \| \overline{\boldsymbol{H}_t} X_i - G_i \|^2] + \lambda \sum_{i=1}^{t} \| H_i \|^2 \} \tag{2}$$

where, $\overline{\boldsymbol{H}_t}$ is a complex conjugate matrix; X_i is the frequency domain of the number i training sample; G_i is the target frequency domain output of the number i training sample; H_i is the frequency domain expression of the optimal correlation filter of the number i training sample.

By combining Equations (1) and (2), Equation (3) was obtained.

$$H_t = \frac{\sum_{i=1}^{t} \overline{G_l} X_i}{\sum_{i=1}^{t} \overline{X_l} X_i + \lambda} \tag{3}$$

where, H_t is the optimal correlation filter.

It can be seen from Equation (3) that the original sample extracted from the detector's target is the total set sampling. Due to a large amount of calculation in the total set sampling, the algorithm's real-time performance is greatly affected. Therefore, a sparse matrix for the cyclic sampling of the target region was used, which can effectively improve the algorithm's computational efficiency. The transform sparse matrix $\boldsymbol{P}$ was used to conduct cyclic sampling on one-dimensional target image x_i=[x_{i1}, x_{i2}, x_{i3}, …, x_{in}, $n \in [1,+\infty)$]. Therefore, the X_i in Equation (3) can be expressed as

$$\boldsymbol{X_i} = \begin{bmatrix} x_{i1} & x_{i2} & \cdots & x_{in} \\ x_{in} & x_{i1} & \cdots & x_{in-1} \\ \vdots & \vdots & \ddots & \vdots \\ x_{i2} & x_{i3} & \cdots & x_{i1} \end{bmatrix} \tag{4}$$

In the process of target tracking, the optimal correlation filter H_t in Equation (3) will constantly update and iterate. For the convenience of expression, the numerator expression in Equation (3) is F_i, while the denominator is L_i. Therefore, the updated expressions of F_i and L_i are as follows:

$$F_i = (1-\theta) F_{i-1} + \theta \sum \overline{G_l} X_i \tag{5}$$

$$L_i = (1-\theta) L_{i-1} + \theta \sum \overline{X_l} X_i \tag{6}$$

where, θ is the learning rate. Therefore, in the next frame of the image, the target position can be obtained by solving the maximum correlation filter response y, and the obtained result is (u, v, w, h). (u, v) is the central pix coordinates of the target; (w, h) is the width and height of the minimum border of the target.

$$y = F^{-1} \left\{ \frac{\sum \overline{F} \boldsymbol{Z}}{L + \lambda} \right\} \tag{7}$$

where, F^{-1} represents the Fourier transform; $\boldsymbol{Z}$ represents the feature matrix of the previous frame.

To keep the tracking for a long time, a support vector machine (SVM) classifier is added to train the effective target samples based on the fusion filter[25] and as an online learning classifier based on this existing KCF algorithm. After the target result is obtained in each frame, the target confidence level is judged: when the target

detection threshold is larger than threshold 1 (th1), it means that the target sample of the frame is positive, and the sample is used as a training sample to train the SVM classifier; When the confidence of the target is smaller than threshold 2 (th2), it means that the target sample of the frame is invalid. At this time, the SVM does not use this sample for training and re-detects the image target. The flow of the improved KCF real-time spot tracking method is shown in Figure 3.

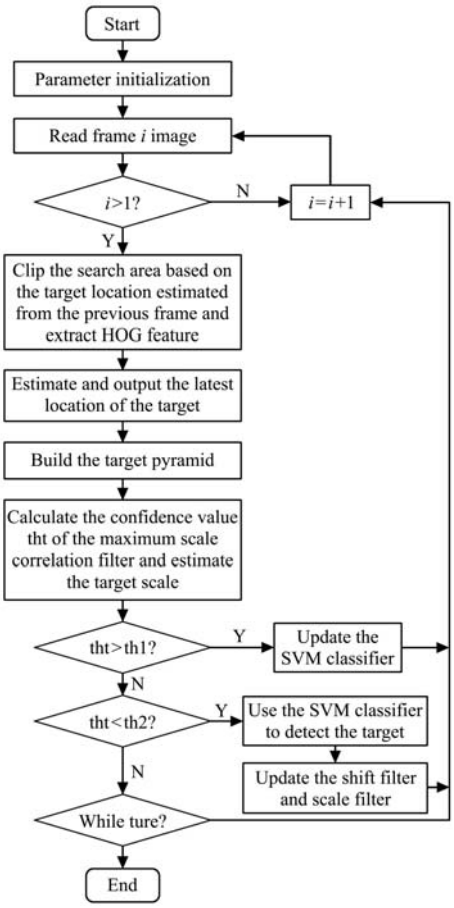

Figure 3 Flow of the improved KCF spot tracking method

When using a pix as a feature, the image is scanned in lexicographical order to form the feature vector. Given N column vector $x_i \in R^d$ and class label $t_i \in \{-1, 1\} \square i \in \{1, 2, 3, \ldots, N\}$, the SVM classifier will find a hyperplane satisfying Equation (8).

$$\begin{aligned} &\min_{w,b} \boldsymbol{w}^T \boldsymbol{w} + C\sum_{i=1}^{N} \varepsilon_i \\ &s.t. t_i(x_i^T w + b) \geq 1 - \varepsilon_i \end{aligned} \tag{8}$$

where, $\boldsymbol{w}^T$ represents the transpose matrix of the matrix $\boldsymbol{w}$; $\boldsymbol{w}$ represents the normal line of the hyperplane; b represents the bias of the hyperplane; ε_i is the relaxation variable; C is the penalty parameter.

4 Navigation control method

4.1 Distance coordinate transformation model

The position coordinate of the spot collected by the CMOS camera is a pix coordinate, which cannot be directly used in actual flight control. Therefore, after obtaining the position information of the target spot in the image plane of the CMOS camera, it is necessary to establish an image coordinate transformation model to convert the pix coordinate (u_0, v_0) of the image into the flight coordinate (X_w, Z_w). Figure 4 is the relationship between pix coordinates and geodetic coordinates.

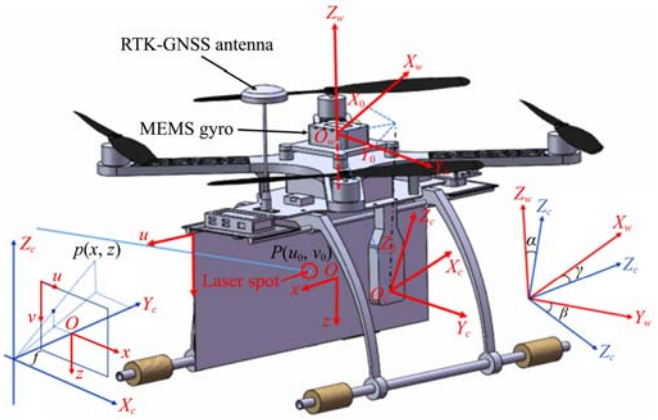

Note: o-uv is the pix coordinate system; o-xz is the image coordinate system; O_c-$X_cY_cZ_c$ is the camera coordinate system; O_w-$X_wY_wZ_w$ is the world coordinate system; P is the laser spot; (u_0, v_0) is the pix coordinates of laser spot.

Figure 4 Image coordinate transformation model diagram

The transformation equation from the image coordinate system to the pix coordinate system is,

$$\begin{bmatrix} u \\ v \\ 1 \end{bmatrix} = \begin{bmatrix} \frac{1}{d_x} & 0 & u_0 \\ 0 & \frac{1}{d_z} & v_0 \\ 0 & 0 & 1 \end{bmatrix} \begin{bmatrix} x \\ z \\ 1 \end{bmatrix} \tag{9}$$

where, u, v are the pix coordinates; d_x is the sum of image units per line; d_z is the sum of image units per column; o-uv is the pix coordinate system; o-xz is the image coordinate system.

The transformation equation from 2D to 3D is,

$$Y_c \begin{bmatrix} x \\ z \\ 1 \end{bmatrix} = \begin{bmatrix} f & 0 & 0 \\ 0 & f & v_0 \\ 0 & 0 & 1 \end{bmatrix} \begin{bmatrix} X_c \\ Z_c \\ Y_c \end{bmatrix} \tag{10}$$

where, X_c, Y_c, and Z_c are the camera coordinates; f is the internal parameter of the camera; x, z is the image coordinate; O_c-$X_cY_cZ_c$ is the camera coordinate system.

The camera coordinate system's transformation to the world coordinate system is mainly the rotation and translation of the camera relative to the ground. The conversion equation is,

$$R = \begin{bmatrix} 1 & 0 & 0 \\ 0 & \cos\alpha & \sin\alpha \\ 0 & -\sin\alpha & \cos\alpha \end{bmatrix} \begin{bmatrix} \cos\beta & 0 & -\sin\beta \\ 0 & 1 & 0 \\ \sin\beta & 0 & \cos\beta \end{bmatrix} \begin{bmatrix} \cos\gamma & -\sin\gamma & 0 \\ \sin\gamma & \cos\gamma & 0 \\ 0 & 0 & 1 \end{bmatrix} \tag{11}$$

$$\begin{bmatrix} X_w \\ Z_w \\ Y_w \end{bmatrix} = R \begin{bmatrix} X_c \\ Z_c \\ Y_c \end{bmatrix} + \begin{bmatrix} X_0 \\ Z_0 \\ Y_0 \end{bmatrix} \tag{12}$$

where, α, β, and γ are the angle of rotation around x, y, and z, respectively; X_w, Y_w, Z_w are the world coordinate; X_0, Y_0, Z_0 are the offsets of the camera for the flight control, O_w-$X_wY_wZ_w$ is the world coordinate system.

Combining Equations (9)-(12), the following is obtained:

$$X_w = |R| \cdot d_x \cdot \frac{Y_c}{f} \cdot (u - u_0) + X_0 \tag{13}$$

$$Z_w = |R| \cdot d_z \cdot \frac{Y_c}{f} \cdot (v - v_0) + Z_0 \tag{14}$$

$$Y_w = |R| \cdot Y_c + Y_0 \tag{15}$$

where, $\frac{Z_c}{f}$ is a CMOS camera internal reference, it is assumed that $d_x \cdot \frac{Y_c}{f}$ and $d_z \cdot \frac{Y_c}{f}$ are the distance coefficients on x, z, respectively.

Since the spot information of the laser receiving device has

only information on two positions, X_w and Z_w, the Y_w position information is ignored. There are Equations (16) and (17) as follows:

$$d_x \cdot \frac{Z_c}{f} = k(d_x) \tag{16}$$

$$d_y \cdot \frac{Z_c}{f} = k(d_y) \tag{17}$$

Substitute Equations (16) and (17) into (13) and (14), Equations (18) and (19) were obtained.

$$X_w = |R| \cdot k(d_x) \cdot (u - u_0) + X_0 \tag{18}$$

$$Z_w = |R| \cdot k(d_z) \cdot (v - v_0) + Z_0 \tag{19}$$

4.2 Gyro-based coordinate information correction algorithm

During the UAVs flight, the laser receiving device will change angle due to the UAVs' attitude angle change. Therefore, the coordinate information correction algorithm based on the gyroscope is proposed to correct the fuselage's tilt interference. The gyroscope used the BMI088 high-performance inertial measurement unit (IMU) produced by Bosch Sensortec. The gyroscope has good paranoid stability (less than 2°/h) and low-temperature coefficient offset (TCO) below 15 mdps/k. While measuring the camera attitude, MEMS gyro-only based system suffers from drift and bias. Therefore, the gyroscope needs to be calibrated. The calibration method of the gyroscope is to place the gyroscope on flat ground and record 5000 sets of data continuously, and calculate the average value of the recorded data as the three-axis zero deviation of the gyroscope. And the gyroscope data with zero offset correction can meet the requirements of camera attitude measurement.

The principle of the body tilt correction algorithm based on the micromachined gyroscope is as follows. The spot position coordinates (X_0, Z_0) output by the CMOS camera are used as the main variables, and the angle of the body (laser receiving device) measured by the UAVs' flight controller gyroscope is used as the correction parameter. The values of (X_w, Z_w) are calculated according to Equations (13) and (14), and then the new coordinate values (X_Δ, Z_Δ) are obtained after the gyroscope angle correction, and the corrected coordinate values are used to participate in the flight control.

Figure 5 depicts conditions of UAVs that have a level or tilted laser receiving device location map; point P is for the laser receiving device that is level in terms of the actual point; P_Δ is the point where the fuselage is tilted and is a laser receiving device to receive the actual point of the same position. As seen from the figure, the fuselage's inclination angle is equal to that of the actual and measured points. Therefore, the relationship between the measured point coordinates and the actual point coordinates is,

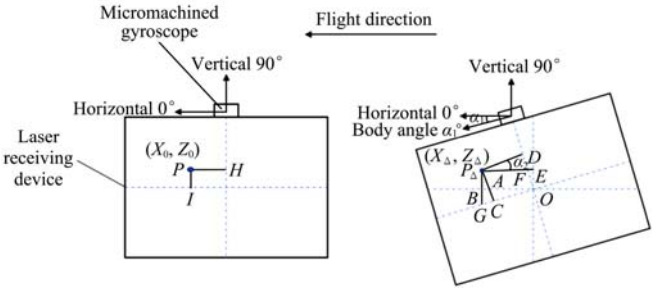

Note: P is the laser spot with angle 0°; (X_0, Z_0) is the position coordinates of spot with angle 0°; P_Δ is the laser spot with angle α_1°; (X_Δ, Z_Δ) is the position coordinates of spot with angle α_1°.

Figure 5 Location of the laser receiver when the UAV is horizontal or tilted

$$X_\Delta = X_0 \cos\alpha_1 - Z_0 \sin\alpha_1 \tag{20}$$

$$Z_\Delta = Z_0 \cos\alpha_1 + X_0 \sin\alpha_1 \tag{21}$$

where, α_1 is the body angle of the UAV.

4.3 Decision control strategy

After the image coordinate conversion and coordinate information correction, it is necessary to establish the relevant flight control method model.

The laser receiving device is divided into four regions: S0, S1, S2, and S3. Figure 6 is the laser receiving device area division diagram. S0 is a non-adjustment zone. When the light spot is on S0, the UAV is in a hovering and self-stabilizing state and does not follow the light spot's position to move. S1 is a buffer zone, which the main function is to gently transition the change of flying speed. When the light spot is above S1, the distance between the nonregulated zones of the light spot is calculated to determine the speed factor and calculate the real-time speed of the UAV at this time. S2 is the adjustment region. When the spot is in this position, the relevant speed calculation formula will be adopted to calculate the speed according to the spot's specific position to realize UAVs' laser tracking. S3 is the off-target adjustment zone. When the spot is in the zone, the spot's specific position cannot be acquired by the laser recognition device. At this time, the UAVs will accelerate flight for 2 s at the previous heading angle.

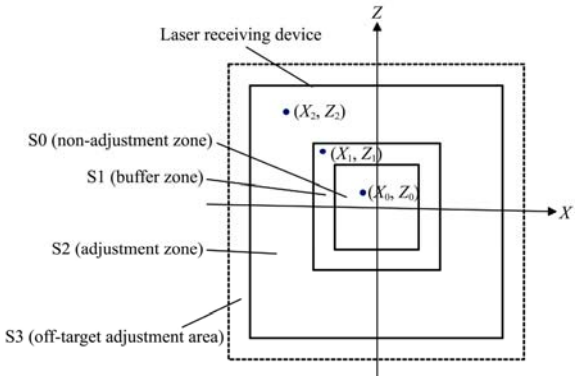

Figure 6 Laser receiving device area division diagram

Different from ordinary filtering, the Kalman filtering method has the advantage of a small delay and can estimate the state of the object in real-time without generating lag. It is widely used in motion estimation, especially in UAV[26]. In this study, the uncontrolled discrete Kalman filter method is adopted to calculate and control UAVs' flying speed when the light spot is in different areas[27].

When the spot is at S1, the coordinate point of the spot at this time is $P_0(X_0, Z_0)$:

$$\overrightarrow{v_{k+1}} = \overrightarrow{v_k} = 0 \tag{22}$$

where, $\overrightarrow{v_k}$ is the velocity at time k; $\overrightarrow{v_{k+1}}$ is the velocity at time k+1.

When the spot is at S2, the coordinate point of the spot is P1 (X_1, Z_1). First, calculate the distance factor Q_x, Q_y:

$$Q_x = \frac{|X_1|}{|X_A|} \tag{23}$$

$$Q_y = \frac{|Z_1|}{|Z_A|} \tag{24}$$

where, (X_A, Z_A) represents the four vertices of the S1 region.

Further, use the uncontrolled discrete Kalman filter method for speed calculation:

$$\overrightarrow{v_1} = \frac{\sqrt{(X_w - X_1)^2 + (Z_w - Z_1)^2}}{T} \tag{25}$$

$$\overrightarrow{v_2} = \overrightarrow{v_k} + \vec{a}T \tag{26}$$

$$k_g = \sqrt{\frac{(v_1 - v_k)^2}{(v_1 - v_k)^2 + (v_2 - v_k)^2}} \tag{27}$$

$$\overrightarrow{v_{k+1}} = \overrightarrow{v_k} + k_g \cdot |\overrightarrow{v_2} - \overrightarrow{v_1}| \tag{28}$$

where, v_1 is the mean square error prediction speed; v_2 is the state prediction speed; k_g is the gain factor; T is the unmanned accelerometer acquisition cycle. (X_w, Z_w) is the position of the spot in an acquisition cycle. a is the UAV acceleration.

Therefore, when the spot is at S2, the speed of the UAV is,

$$v_{k+1(x)} = Q_x \cdot |v_{k+1}| \cdot \frac{x}{\sqrt[2]{x^2 + z^2}} \tag{29}$$

$$v_{k+1(y)} = Q_y \cdot |v_{k+1}| \cdot \frac{y}{\sqrt[2]{x^2 + z^2}} \tag{30}$$

$$v_{k+1(z)} = 0 \tag{31}$$

When the spot is at S2, the coordinate point of the spot is P_2 (X_2, Z_2). At this time, the UAV moves completely following the spot, and P_2 is brought into Equations (25)-(28).

$$v_{k+1(x)} = |v_{k+1}| \cdot \frac{x}{\sqrt[2]{x^2 + z^2}} \tag{32}$$

$$v_{k+1(z)} = |v_{k+1}| \cdot \frac{z}{\sqrt[2]{x^2 + z^2}} \tag{33}$$

When the spot is at S3, the laser receiving device has lost the spot at this time, and the spot has no coordinates. At this point, the follower continues to fly at the heading angle and acceleration before the light spot disappears to find the laser spot. At this time, the UAV speed is,

$$v_{k+1} = v_k + aT \tag{34}$$

If no spot is found, the speed drops to 0 and enters the hovering state. The speed is now,

$$v_{k+1} = 0 \tag{35}$$

5 Experiment and results

5.1 UAVs for test

As the F450 quad-axis UAV is flexible and small, capable of carrying a large load, and has a long endurance, this study chose the F450 quad-axis UAV as the test UAV platform. Its main parameters are listed in Table 4. In navigation and positioning devices, both leader and follower use airborne optical flow sensors and ultrasonic sensors for auxiliary positioning. The leader uses manual operation to control the flight, and the follower realizes the automatic flight function according to the laser tracking system. To accurately describe UAV's trajectory, RTK was used to record UAVs' position. RTK is a NEO-M8P RTK-GNSS module produced by Ublox. The base station is a mobile base station, and the positioning accuracy of the airborne mobile station is centimeter-level and relative coordinates.

Table 4 Main specifications of test UAV

Parameter	Unit	Value
Supply mode	mAh	3S lithium battery, 5300 mAh
Dimensions	mm	370 mm×370 mm×240 mm
payload	kg	1 kg
endurance	min	20 min
Number of propellers		4
Location mode (follower)		Optical flow sensor and ultrasonic sensor
Location mode (leader)		Optical flow sensor and ultrasonic sensor
RTK		Centimeter accuracy
MEMS gyro		6-axis, Sensitivity:16.4 LSB/(°)·s^{-1}

According to the previous design scheme, an automatic navigation device for a UAV based on laser tracking is fabricated. Figure 7 shows a physical diagram of the overall device.

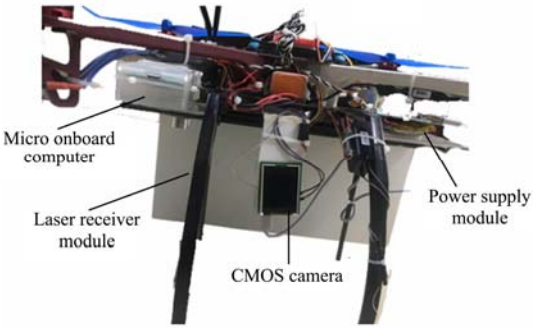

a. Follower UAV equipped with laser tracking system

b. Leader UAV equipped with laser tracking system

Figure 7 Physical diagram of the overall device

5.2 Distance model calibration experiment

The calibration experiment procedure is as follows: taking the intersection of the laser receiving device and the CMOS camera as the origin, vertical lines and horizontal dotted lines are formed on the laser receiving device, and the distance Δx between the adjacent two points is 0.5 cm. The laser receiving device and the CMOS camera are fixed on the ground, and the laser transmitting device fires laser beam at different positions to irradiate the laser receiving device. The pix coordinates $O(0, v)$ of the vertical point of the pix coordinate $A(u, 0)$ of the lateral point and the actual camera coordinate $W(x, z)$ are recorded, and the above experimental steps are repeated thirty times. The average pix coordinates and the average camera coordinates corresponding to each point are substituted into Equations (13) and (14) to solve the corresponding parameters. Figure 8 shows the calibration experiment diagram of the distance relationship between pixel coordinate and image coordinate.

As shown in Figure 9, the difference in the position change of the spot changes correspondingly with the distance between the laser receiving device and the CMOS camera. When the distance is 8 cm, the average difference of the horizontal pix coordinates is 118.2 pix/cm, and the average difference of the vertical pix coordinates is 114.2 pix/cm. When the distance is 24 cm, the average difference of the horizontal pix coordinates is 45.5 pix, and the average difference of the vertical pix coordinates is 46.5 pix. Therefore, linear, logarithmic, quadratic, and exponential curves fit the distance between the laser receiving device and the CMOS camera in horizontal and vertical coordinates. In the horizontal pix coordinate curve fitting, the quadratic curve has R^2=0.9969, and the matching degree and saliency are better than other curves. The fitting curve is $k(d_x)=0.415d^2-19.1d+261.5$. In the vertical pix coordinate curve fitting, the quadratic curve has R^2=0.9729, and the matching degree and saliency are better than other curves. The fitting curve is $k(d_z)=0.231d^2-11.9d+200.8$. Figure 10 is a

curve fit diagram of horizontal and vertical pix. The fitted curve and the known parameters u_0=320, v_0=240, and the mounting dimension α=90°, β=0°, γ=0°, X_0=5 cm, Z_0=3 cm are substituted into Equations (18) and (19), and the equations as follows were obtained:

$$X_w=(0.14d^2-6.58d+103.18)\cdot(u-320)+5 \quad (36)$$

$$Z_w=(0.11d^2-5.34d+90.96)\cdot(v-240)+3 \quad (37)$$

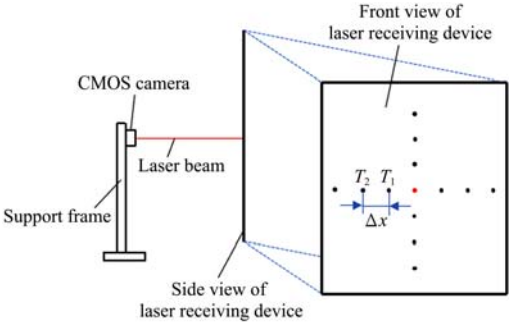

a. Experiment hint diagram

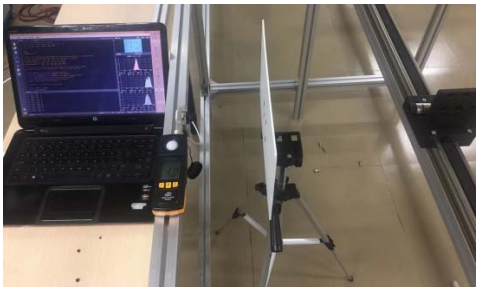

b. Experiment entity diagram

Figure 8 Calibration experiment diagram of distance relationship between pixel coordinate and image coordinate

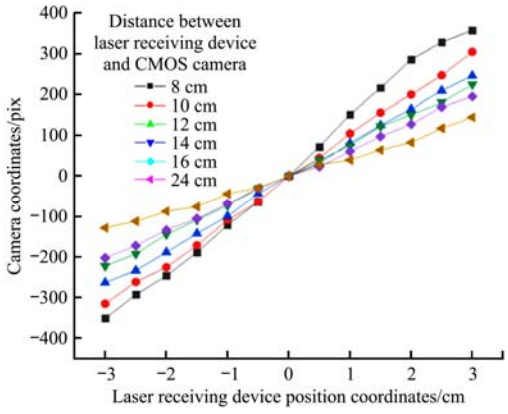

a. Horizontal coordinate

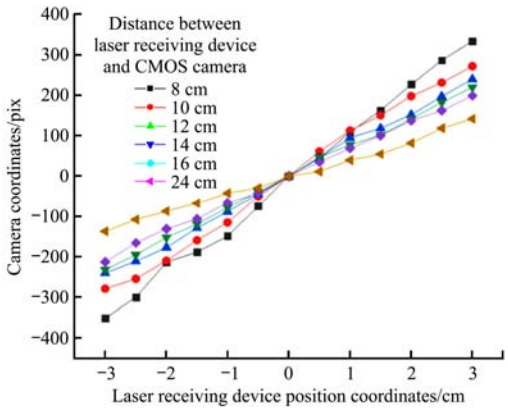

b. Vertical coordinate

Figure 9 Relationship between spot coordinates and actual coordinates at different distances

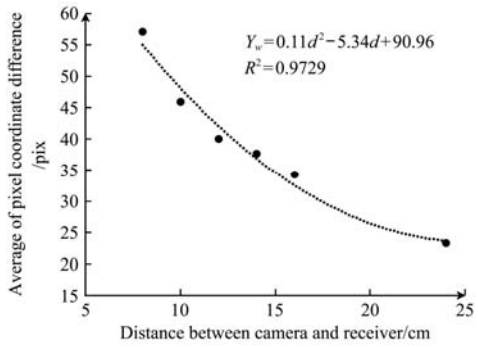

a. Horizontal coordinate

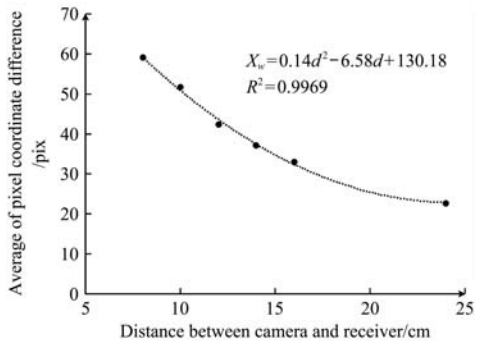

b. Vertical coordinate

Figure 10 Curve fitting map of adjacent coordinate pix under different distances

5.3 Spot recognition experiment with different illumination brightness

The experiment procedure is as follows: Install the fixed support frame and fix the CMOS camera and the laser receiving device in a relative position. Add impurities with the same or similar color as the laser spot on the laser receiving device and within the visible range of the CMOS camera as the interference source 1, and add impurities with the same or similar color as the soil as the interference source 2, as shown in Figure 11. The laser receiving device was placed under 12 luminance levels of 15.4 lx, 27.6 lx, 37.8 lx, 39.4 lx, 71.4 lx, 149.6 lx, 161.8 lx, 192.2 lx, 199.8 lx, 213.2 lx, 35 600 lx, and 48 500 lx. The first ten of them were indoor illumination, and the last two were outdoor illumination. The laser transmitting device is used to illuminate the laser receiving device and remains stationary. The classical KCF algorithm is used to compare the recognition effect with the improved KCF algorithm. After completing the stationary recognition, control the light spot to move between (−3, 0), (3, 0) and (0, −3), (0, 3) and the moving speed is set to 0.2 m/s, 0.4 m/s, 0.6 m/s, 0.8 m/s, 1.0 m/s. Use the classic KCF algorithm to compare the tracking effect with the improved KCF algorithm in this study, record the recognition of light spots in the video stream every second within 1 min, and count the light spot's recognition rate.

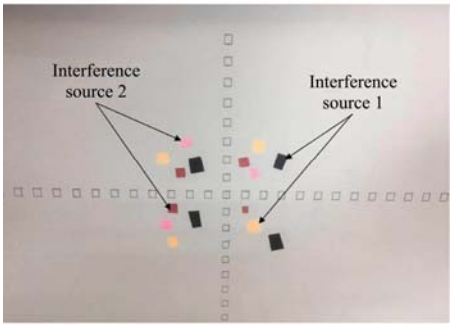

Figure 11 Laser receiving device with interference source

As shown in Figure12a, when the illumination brightness is low, the classical KCF algorithm shows incomplete target contour detection and over-segmentation of the target in different degrees. When the illumination brightness is 71.4 lx, the classical KCF algorithm recognizes the artificially added interference source in the target contour. When the light intensity is 149.6 lx, and the indoor light is above this value, the classical KCF can identify the target contour more accurately. When the laser receiving device and transmitting device are placed in the outdoor light, the classical KCF algorithm will lose the target due to the high outdoor light intensity and the influence of outdoor natural light. It can be seen from Figure 12b that when the ambient light intensity is low, the optimized recognition algorithm can effectively recognize the light spot. As the brightness increases, the algorithm can effectively reduce the impact of light intensity and identify the location of the light spot. Simultaneously, when the lighting conditions are outdoor natural light, the recognition algorithm can accurately identify the target spot and maintain good target detection ability.

As shown in Figure13a, when the classical KCF algorithm is adopted, the contrast between the laser spot and the laser receiving device is relatively bright at the low illumination luminance of 15.4 lx and 27.6 lx, so its recognition rate is relatively high, with the highest recognition rate reaching 75%. When the laser receiving device is in high outdoor light intensity, the highest target tracking rate is only 20% because the laser spot cannot be correctly identified. Due to the influence of natural light, the identification results will be wrong. As shown in Figure 13b, under different illumination luminances, the laser transmitting device adopts different moving speeds. The algorithm of this study can maintain relatively high tracking accuracy, with an average tracking accuracy above 95%. Therefore, by comparing the above two experiments, the improved algorithm has strong robustness regarding the influence of illumination brightness and target movement speed. The tracking effect in the process of color target movement is better than the classical KCF algorithm.

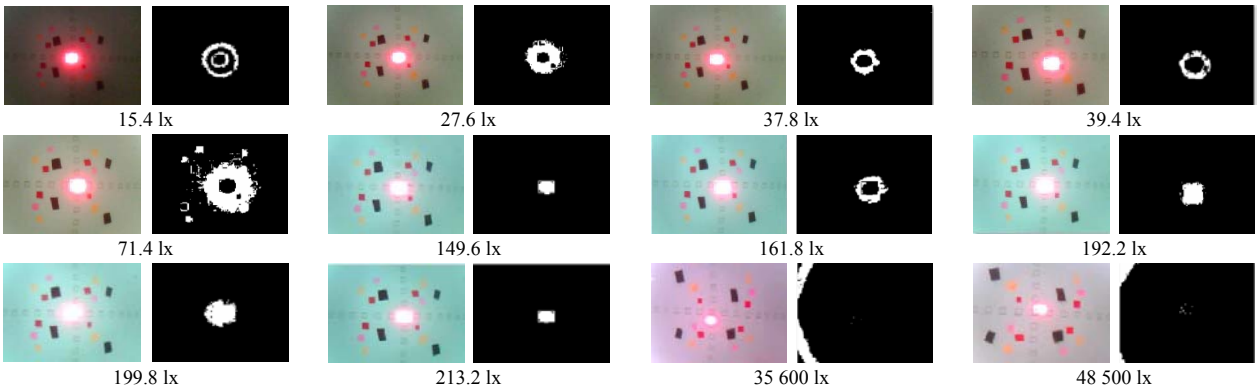

a. Original and identification diagrams of classical algorithms

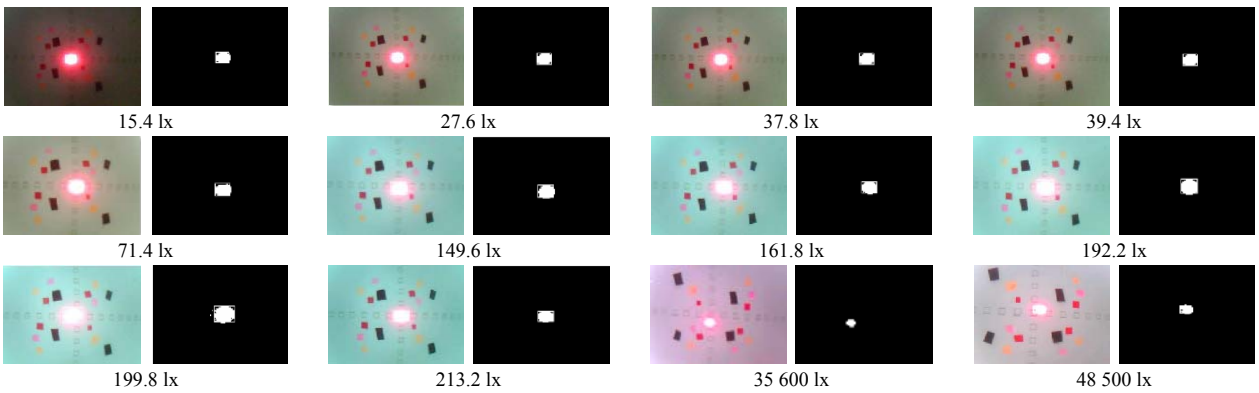

b. Original and identification diagrams of optimization algorithms

Figure 12 Two algorithms of identification and contrast under different brightness conditions

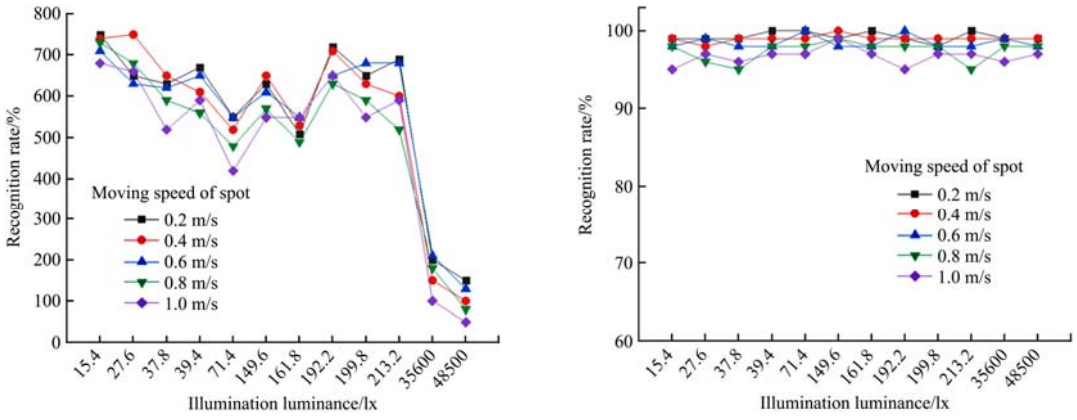

a. Classical algorithm b. Optimization algorithms

Figure 13 Recognition rate of dynamic spots

5.4 Calibration experiment for static body tilt interference

An interference correction experiment in a static environment is conducted to verify the micro-gyroscope coordinate algorithm's accuracy. The experiment procedure is as follows: firstly, fix the laser transmitting device on the flat ground and fix the laser receiving device and CMOS camera in relative positions. Secondly, adjust the relative positions of the transmitting device and receiving device so that the CMOS camera can collect the spot's position information on the receiving device during the angle adjustment. Finally, compare the coordinate errors before and after correction. Figure 14 is the angle (α) of laser receiving device. A total of 7 tilting laser receiving devices at different angles of 5°, 10°, 15°, 20°, 25°, and 30° were simulated, and the position information of light spots collected by the laser recognition device was recorded, as listed in Table 5. The calculation equation of coordinate error is as follows:

$$\Delta X=X_\alpha-X_0 \quad (38)$$

$$\Delta Z=Z_\alpha-Z_0 \quad (39)$$

Table 5 Data comparison before and after tilting interference correction of UAV

Angle /(°)	Actual location /cm	Precorrection error/cm	Correction value/cm	Corrected error/cm
0	(8.40,4.00)	(0, 0)	(8.40,4.00)	(0, 0)
5	(8.02,4.71)	(0.38, 0.71)	(8.37,4.12）	(−0.13,0.12)
10	(7.57,5.39)	(0.83, −1.40)	(8.41,4.05）	(0.11,0.15)
15	(7.08,6.04)	(1.32, -2.04)	(8.43,3.98）	(0.13, 0.12)
20	(6.53,6.63)	(1.87, −2.63)	(8.42,4.01）	(0.12,0.11)
25	(5.92,7.17)	(2.47, −3.17)	(8.42,4.03）	(0.12,0.13)
30	(5.27,7.66)	(3.12, −3.66)	(8.44,3.98）	(0.14, 0.12)

As seen in Table 5, when the laser receiving device is not subject to tilt interference (inclination angle is 0°), the spot's position information is (8.40, 4.00) cm. After the tilt interference, the position information of the spot changes and gradually decreases. After calibration according to the gyroscope angle, the maximum error of the spot position is reduced from the pre-correction (3.12, −3.66) cm to the post-correction (0.14, −0.12) cm. It can be seen that an improved algorithm can better eliminate the interference error caused by the tilt of the laser receiving device caused by the tilt of the fuselage of the UAVs during flight.

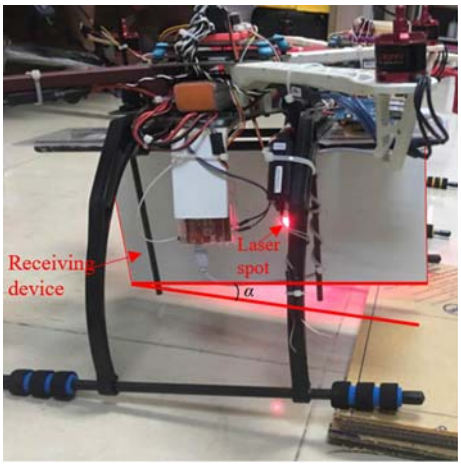

Figure 14 Angle (α°) of laser receiving device

5.5 Automatic collaboration of two UAVs

After the above experiments, it is necessary further to test the tracking device's space tracking effect. A flight experiment is conducted in the school playground at 4 pm, and the weather was a breeze. The laser transmitting device is installed in the leader; the laser receiving device and laser recognition device are installed in the follower. During the flight, the two UAVs' horizontal distance is kept to 2 m and locked in the horizontal position. After completing the laser tracking system's calibration, the leader and follower take off to 1.5 m. Waiting for two UAVs to stably hover, the leader turns on the laser transmitting device and fires a laser beam, the laser receiving device receives the leader's laser and forms a spot, laser recognition device begins gathering spot location information. The leader starts to fly according to the pre-designed flight path, and the maximum flying speed is 2 m/s. The follower fly tracked according to the location of the spot. Figure 15 is the actual flying diagram of leader and follower tracking.

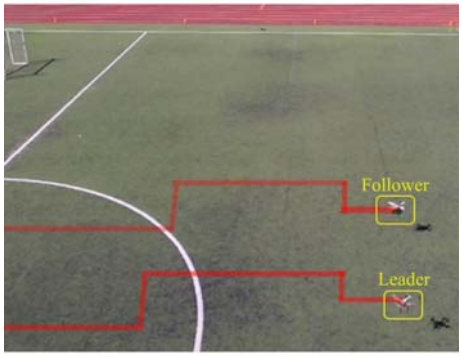

Figure 15 Leader and follower tracking flight

Figure 16a is the three-dimensional trajectory of the leader and follower tracking flight and the leader's preplanned flight path. Figure 16b is the projection of the flight trajectory in the *X*-*Z* plane. It can be seen from Figure 16b that when the leader flies in a straight line, the follower can better track the flight of the leader. However, when the current leader turns, the follower's movement trajectory error is relatively large, such as point 1-7. During the hover at point 1, the follower deviated in both the *X*- and *Z*-directions, possibly due to wind interference in the sky. When it comes to point 2-7, the deviation is mainly caused by the flying speed control method adopted in the tracking flight in this paper, instead of using the coordinates of geographical position information to control the UAV for tracking the flight. Therefore, in fast flight, the movement distance of followers will exceed the leader's position due to the UAV's fast braking. However, the average return time of the seven inflection points was 0.83 s.

Figure 17 shows the absolute error change of the trajectory of the follower relative to the trajectory of the master during the entire tracking process. It can be seen that during the flight, the absolute error reaches the maximum error at 140 s, which is 17.2 cm. However, the absolute error of the flight trajectory has some jump noise. The main reason is the jump noise generated by the flight decision mode of the light spot in different regions of the laser receiving device. When the light spot is in the non-adjustment zone of the rectangle, the follower uses the airborne sensor to adjust the hover stably. And due to the small size of the UAV frame, there is interference from the natural wind during the flight, which causes the tracking trajectory parameters to drift, and the trajectory error has jumping noise. When the leader is flying straight from point 1 to point 2 in Figure 16b, the follower will fly synchronously according to the position of the light spot. Due to the change of the attitude angle during the flight, the UAV has a height change in the vertical direction. When the accumulated height deviation exceeds the boundary of the non-adjustment zone,

the light spot will enter the buffer zone in the vertical direction. At this time, the laser tracking system will adjust the corresponding speed in the vertical direction, so that the light spot returns to the no-adjustment zone in the laser receiving device. Due to the change of the attitude of the follower and the existence of factors of flight decision during the flight, the tracking error of the follower is caused as shown in Figure 17. However, it can be seen from the figure that the average tracking error of the follower remains around 6 cm. Compared with the existing visual tracking methods[13,15], the method proposed in this study has better tracking ability.

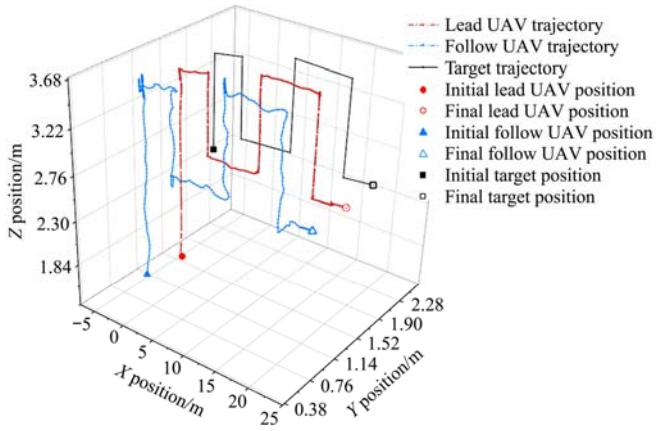

a. Three-dimensional trajectory

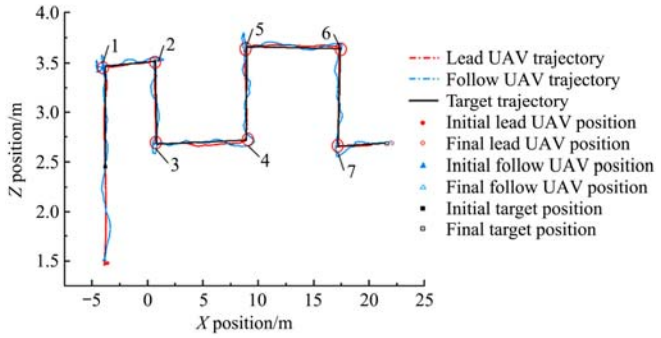

b. Two-dimensional trajectory

Figure 16 Leader and follower tracking flight trajectory

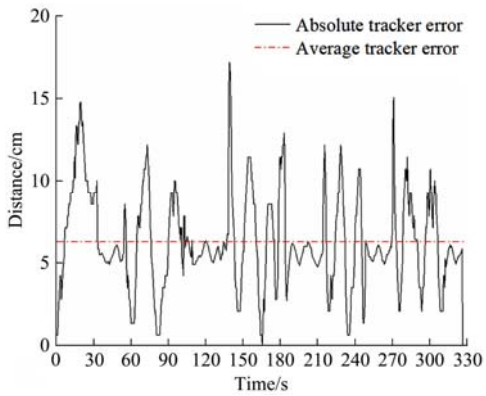

Figure 17 Error variation in the whole process

As listed in Table 6, the relative offset between the follower tracker and the leader tracker is analyzed, from which it can be seen that in the *X*-axis direction, the average offset is 5.2 cm, and the coefficient of variation is 0.0181. In the *Z*-axis direction, the average offset is 7.3 cm, and the coefficient of variation is 0.0414. Compared with the *X*-axis offset, the *Z*-axis direction of the average deviation, maximum deviation, and variation coefficient were greater than in the *X*-direction. The main reason is that there has a natural lateral drift effect of UAVs in the *Z*-direction during flight, and in the *X*-direction, flying UAVs have inertia; therefore, the natural wind has a smaller influence on the flight in the *X*-direction. From the analysis of the whole trajectory, it can be concluded that the average deviation of the whole trajectory is 6.3 cm, and the variation coefficient is 0.0297. Therefore, the device in this study has high reliability when applied to UAVs.

Table 6 Trajectory analysis parameters

Direction	Average offset /cm	Maximum offset/cm	Coefficient of variation
X-direction	5.2	8.8	0.0181
Z-direction	7.3	17.2	0.0414
Full track	6.3	13.0	0.0297

6 Conclusions

In this study, a novel cooperative navigation method was proposed for two UAVs based on laser tracking and the design of a laser tracking system, which successfully combines laser tracking and visual navigation. According to the function requirement, each part of the system was designed and researched. Based on the above experimental analysis results, the following conclusions can be made:

1) In view of the difference in the unit displacement of the light spot between the camera and the laser receiving device at different installation distances, a correlation between the installation distance and the unit displacement was established on the *X*-axis and the *Z*-axis. The coefficients R^2 of the quadratic fitting curve of the *X*-axis and *Z*-axis are 0.9969 and 0.9729 respectively, which can effectively eliminate the influence of the installation distance on the actual movement distance of the light spot.

2) Aiming at the problem of unstable spot recognition due to changes in lighting conditions, and improved KCF real-time spot tracking method was proposed. A scale filter was added based on the displacement filter, sparse matrix cyclic sampling was used instead of full sampling, and SVM was added for online learning of target samples. The improved recognition algorithm can accurately identify the position coordinates of the related light spots when there are multiple interference sources. At the same time, compared with the traditional KCF recognition algorithm, the recognition algorithm in this study can effectively track the light spot under 12 different illumination conditions. Under indoor lighting conditions, the tracking recognition rate of the light spot has increased from 70% to 95%. Under outdoor conditions, the tracking recognition rate of the light spot has increased from 20% to 90%. The experimental results show that the identification and tracking algorithm can effectively reduce the influence of light conditions and interference sources, and has strong robustness.

3) Aiming at tilt interference, a correction algorithm based on a micromachined gyroscope was designed. When the fuselage is tilted 30°, the error is reduced from (3.12, −3.66) cm before correction to (0.14, 0.12) cm after correction. It can better eliminate the interference error of the laser receiving device tilt caused by the tilt of the fuselage of the UAV during the flight.

4) In the outdoor flight experiment of two UAVs, the follower can accurately track the leader for synchronized flight. Comparing the flight trajectories of leader and follower, the average deviation of the two UAVs on the *X*-axis is 5.2 cm, and the coefficient of variation is 0.0181; the average deviation on the *Z*-axis is 7.3 cm, and the coefficient of variation is 0.0414. The experiment results show that the system can accurately realize the

synchronous flight of two UAVs.

The outdoor flight experiment has proved that the tracking system is effective and can reduce the impact of complex lighting conditions and changeable illumination conditions on the visual tracking of UAVs, and achieve stable simultaneous flight of two UAVs. Compared with the existing multi-UAV vision collaboration navigation[13,15], the system in this study has higher accuracy and higher robustness and provides a new navigation method based on optical tracking for multi-UAVs cooperative navigation. But in the process of tracking the flight of the system the follower's trajectory still has jumping noise, and the flight stability of the follower needs to be improved. Therefore, more work would be done in optimizing the method of receiving light spots and flight strategy after receiving the laser. In the following research, the agricultural UAV will be used to carry out a large region of outdoor flight experiments.

Acknowledgments

This work was supported in part by the Laboratory of Lingnan Modern Agriculture Project (Grant No.NT2021009), in part by the Science and Technology Plan of Jian City of China (Grant No. 20211-055316); in part by the National Natural Science Foundation of China (Grant No. 31871520); in part by the Science and Technology Plan of Guangdong Province of China (Grant No. 2021B1212040009,2017B090903007), in part by the Guangdong Basic and Applied Basic Research Foundation under (Grant No. 2020A1515110214), and in part by Innovative Research Team of Agricultural and Rural Big Data in Guangdong Province of China under (Grant No. 2019KJ138). The authors wish to thank sincerely the editors and anonymous reviewers for their critical comments and suggestions to improve the manuscript.

[References]

[1] Fan B K, Li Y, Zhang R Y, Fu Q Q. Review on the technological development and application of UAV systems. Chinese Journal of Electronics, 2020; 29(2): 199–207.

[2] Xue X Y, Lan Y B, Sun Z, Chang C, Hoffmann W C. Develop an unmanned aerial vehicle based automatic aerial spraying system. Computersand Electronics in Agriculture, 2016; 128: 58–66.

[3] Faical B S, Freitas H, Gomes P H, Mano L Y, Pessin G, de Carvalho A C P L, et al. An adaptive approach for UAV-based pesticide spraying in dynamic environments. Computersand Electronicsin Agriculture, 2017; 138: 210–223.

[4] Saeed A S, Younes A B, Islam S, Dias J, Seneviratne L, Cai G. A review on the platform design, dynamic modeling and control of hybrid UAVs. In: 2015 International Conference on Unmanned Aircraft Systems (ICUAS), Denver, USA: IEEE, 2015; pp.806–815. doi: 10.1109/ICUAS.2015.7152365.

[5] Xu C C, Liao X H, Tan J M, Ye H P, Lu H Y. Recent research progress of unmanned aerial vehicle regulation policies and technologies in urban low altitude. IEEE Access, 2020; 8: 74175–74194.

[6] Causa F, Vetrella A R, Fasano G, Accardo D. Multi-UAV formation geometries for cooperative navigation in GNSS-challenging environment. In: 2018 IEEE/ION Position, Location and Navigation Symposium (PLANS), Monterey, USA, 2018; pp.775–785. doi: 10.1109/PLANS.2018.8373453.

[7] Karrer M, Agarwal M, Kamel M, Siegwart R, Chli M. Collaborative 6DoF relative pose estimation for two UAVs with overlapping fields of view. In 2018 IEEE International Conference on Robotics and Automation (ICRA), Brisbane, Australia: IEEE, 2018; pp.6687–6693. doi: 10.1109/ICRA.2018.8461143.

[8] Spurny V, Baca T, Saska M, Penicka R, Krajnik T, Thomas J, et al. Cooperative autonomous search, grasping, and delivering in a treasure hunt scenario by a team of unmanned aerial vehicles. Journal of Field Robotics, 2019; 36(1): 125–148.

[9] Pan R H, Xu S H. Multi-UAV cooperative navigation algorithm based on geometric characteristics. Journal of Ordnance Equipment Engineering, 2017; 10: 55–59. (in Chinese)

[10] Guo K X, Li X X, Xie L H. Ultra-wideband and odometry-based cooperative relative localization with application to multi-UAV formation control. IEEE Transactions on Cybernetics, 2020; 50(6): 2590–2603.

[11] Jongug C, Yudan K. Fuel-efficient three-dimensional controller for leader-follower UAV formation flight. In: 2007 International Conference on Control Automation and Systems, Seoul: IEEE, 2007; pp.806–811. doi: 10.1109/ICCAS.2007.4407011.

[12] Ivanov L I, Obukhova N A, Baranov P S. Review of modern UAV detection algorithms using methods of computer vision. In: 2020 IEEE Conference of Russian Young Researchers in Electrical and Electronic Engineering (EIConRus), St. Petersburg and Moscow: IEEE, 2020; pp.322–325. doi: 10.1109/EIConRus49466.2020.9039352.

[13] Tang Y Z, Hu Y C, Cui J Q, Liao F, Lao M J, Lin F, et al. Vision-aided multi-UAV autonomous flocking in GPS-denied environment. IEEE Transactions on Industrial Electronics, 2019; 66(1): 616–626.

[14] Kalal Z, Mikolajczyk K, Matas J. Tracking-learning-detection. IEEE Transactions on Software Engineering, 2011; 34(7): 1409–1422.

[15] Lin F, Mao P K, Xu D X, Yu Z S, M C B. Vision-based formation for UAVs. Taichung: IEEE, 2014; pp.1375–1380. doi: 10.1109/ICCA.2014.6871124.

[16] Vetrella A R, Causa F, Renga A, Fasano G, Accardo D, Grassi M. Flight demonstration of multi-UAV CDGPS and vision-based sensing for high accuracy attitude estimation. In: 2017 International Conference on Unmanned Aircraft Systems (ICUAS), Miami: IEEE, 2017; pp.237–246. doi: 10.1109/ICUAS.2017.7991378.

[17] Gassner M, Cieslewski T, Scaramuzza D. Dynamic collaboration without communication: Vision-based cable-suspended load transport with two quadrotors. In: 2017 IEEE International Conference on Robotics and Automation (ICRA), Singapore: IEEE, 2017; pp.5196–5202. doi: 10.1109/ICRA.2017.7989609.

[18] Yan L, Fang L F, Wei Z. A study on the sync guidance of the multi-lasers with the micro-vision. In: The 26th Chinese Control and Decision Conference (2014 CCDC), Changsha: IEEE, 2014; pp.1449–1453. doi: 10.1109/CCDC.2014.6852395.

[19] Walter V, Staub N, Franchi A, Saska M. UVDAR system for visual relative localization with application to leader-follower formations of multirotor UAVs. IEEE Robotics and Automation Letters, 2019; 4(3): 2637–2644.

[20] Park H, Choi I, Park S, Choi J. Leader-follower formation control using infrared camera with reflective tag. In: 2013 10th International Conference on Ubiquitous Robots and Ambient Intelligence, Jeju, Korea: IEEE, 2013; pp.321–324.

[21] Fang F, Qian K, Zhou B, Ma X. Real-time RGB-D based people detection and tracking system for mobile robots. In: 2017 IEEE International Conference on Mechatronics and Automation (ICMA), Takamatsu, Japan: IEEE, 2017; pp.1937–1941. doi: 10.1109/ICMA.2017.8016114.

[22] Xiang C, Mao J. Research on target detection method based on HSV fusion Gaussian mixture model. In: 2019 3rd International Conference on Electronic Information Technology and Computer Engineering (EITCE), Xiamen, China: IEEE, 2019; pp.327–331. doi: 10.1109/EITCE47263.2019.9094782.

[23] Janousek J, Marcon P, Pokorny J, Mikulka J. Detection and tracking of moving UAVs. In: 2019 PhotonIcs & Electromagnetics Research Symposium - Spring (PIERS-Spring), Rome: IEEE, 2019; pp.2759–2763. doi: 10.1109/PIERS-Spring46901.2019.9017351.

[24] Henriques J F, Caseiro R, Martins P, Batista J. High-speed tracking with kernelized correlation filters. IEEE Transactions on Pattern Analysis and Machine Intelligence, 2015; 37(3): 583–596.

[25] Li Q, Liu L, Ma X, Chen S, Yun H, Tang S. Development of multitarget acquisition, pointing, and tracking system for airborne laser communication. IEEE Transactions on Industrial Informatics, 2019; 15(3): 1720–1729.

[26] Luo Y, Ye G, Wu Y, Guo J, Liang J, Yang Y. An adaptive Kalman filter for UAV attitude estimation. In: 2019 IEEE 2nd International Conference on Electronic Technology (ICET), Chengdu: IEEE, 2019; pp.258–262. doi: 10.1109/ELTECH.2019.8839496.

[27] Lee D H, Lee S S, Kang H H, Ahn C K. Camera position estimation for UAVs using SolvePnP with Kalman filter. In: 2018 1st IEEE International Conference on Hot Information-Centric Networking (HotICN), Shenzhen: IEEE, 2018; pp.250–251. doi: 10.1109/HOTICN.2018.8606037.